



# Numerical Studies on the Creep Behavior of Shear Endplate Connection Assemblies UNDER Transient Heating

*Hadi O. Al Haddad, Elie G. Hantouche\* and Karim K. Al Khatib, Department of Civil and Environmental Engineering, American University of Beirut, PO Box 11-0236, 1107 2020 Riad El-Solh, Beirut, Lebanon*

**Received:** 5 November 2018/**Accepted:** 25 April 2019

**Abstract.** Correct assessment of the steel connection performance under fire requires including the time-dependent response of steel material in the structural analysis. Failure to do so might impose critical threats on the stability and integrity of steel structures. To this aim, the objective of this study is to investigate the effect of thermal creep on the behavior of shear endplate beam-column connections subjected to transient-state fire temperatures. First, finite element models of shear endplate assemblies are developed using ABAQUS and validated against experimental work available in the literature. Parametric studies are then carried out to study the effect of key geometrical, thermal, and material parameters on the overall response of the frame assembly in fire while explicitly including creep. This includes heating and cooling rates, initial cooling temperature, column size and height, load ratio, plate thickness, and steel grade. The results show that including thermal creep causes a reduction in the induced compressive forces and an increase in the mid-span beam deflection, for about six times higher in some cases, thus earlier development of beam catenary action. It is also concluded that lower heating and cooling rates result in larger beam tying forces on the shear end plate connections, which can reach values around ten times larger than when creep is neglected. This study shows that the current practice of neglecting creep in fire analyses, especially in slow heating, may underestimate the forces that are exerted on the shear endplate connections during fire and thus leads to unsafe structural design.

**Keywords:** Shear endplate, Thermal creep, Fire, Finite element, Steel, Transient-state

## 1. Introduction

Steel connections have a critical role in maintaining the overall structural stability by ensuring a continuous load path between connected elements. Specifically, shear endplate connections, also known as flexible endplate connections, are commonly designed as pinned connections that sustain gravitational loads only. However, such connections undergo significant loss of stiffness and strength during fires [1]. In addition, substantial axial stresses develop near the connection region

---

\* Correspondence should be addressed to: Elie G. Hantouche, E-mail: [eh12@aub.edu.lb](mailto:eh12@aub.edu.lb)



because of the restrained thermal expansion of the steel beam. The level of the beam end restraint is determined by the column flexural stiffness. During heating, these axial forces are compressive at first [2]. Yet, at late stages of fire, the excessive beam sagging causes a change in the beam axial forces from compression to tension, also known as beam catenary action. During the cooling stage, additional tension develops in the connection because of the beam thermal contraction. Thus, the large deformations and the additional force demands combined with steel strength degradation can lead to failure during fire events. Extensive research work was done by Luecke et al. [3] to investigate the collapse of the World Trade Center on September 11, 2001. It was recognized that the fire resistance of steel is time-dependent and thus the so-called thermal creep of steel was included in all the FE simulations.

### ***1.1. Time-Independent Analysis***

Several experimental studies were conducted in an attempt to understand the shear endplate connections' behavior when exposed to fire. Wang et al. [4] studied the robustness of different steel connections in fire, including shear endplates. For each connection type, two tests were performed using different column sizes to represent different end restraints. It was found that the shear endplate connection performed the poorest while extended endplate performed the best in terms of ductility and tying force capacity. Moreover, Hu et al. [5] investigated isolated shear endplate strength using experimental and analytical methods. They identified shear endplate rupture at the toe of the weld as the governing mode of failure.

Numerical investigation has proven to be a reliable approach to investigate the behavior of steel connections in fire by closely predicting the experimental results. Using FE models, Hantouche and Sleiman [6] compared double angle with shear endplate connections when exposed to elevated temperatures. Beam web and lower flange buckling, along with failure in tension bolts, were the observed failure modes in the studied shear endplate models. Moreover, Hantouche and Sleiman [7] investigated key parameters influencing isolated shear endplate connections numerically and proposed a mechanical model to estimate the time-independent behavior of shear endplates subjected to fire. Several studies have shown that steel behaves differently when subjected to different fire scenarios [8]. The current state of the art work on numerical studies did not account for the time-dependent behavior of steel such as thermal creep behavior.

### ***1.2. Time-Dependent Analysis***

Thermal creep strain in structural steel is the time-dependent inelastic strain that results from both high temperatures and stresses. This phenomenon is commonly observed when the temperature in steel exceeds one-third to half its melting temperature. Creep, represented in strain versus time curves, consists of three stages: primary, secondary, and tertiary. A non-linear curve with a reducing creep strain rate characterizes the primary phase. Then, the creep strain rate is nearly constant in the secondary stage, whereas it develops rapidly with time in the tertiary stage until failure occurs. Note that creep curves vary depending on the material prop-

erties, temperatures, and stress levels in steel [9]. Thermal creep can be included either implicitly in the material stress–strain curves or explicitly through a subroutine that incorporates a predefined constitutive creep model. In the literature, implicit consideration of creep is widely used by researchers for its availability in codes and standards [10], ease of implementation, and low computational cost.

The majority of the fire experiments available in literature were conducted under standardized fire curves that are not necessarily representative of building fires. Following these *fast* fire curves in the fire tests prohibits creep strains from developing. This explains the satisfactory results obtained by using the implicit method when reproducing the experimental work. However, Kodur and Dwaikat [11] realized that considering creep explicitly is closer to the real behavior of steel in fire. In addition, one of their findings was that implicit considerations could partially account for creep and thus yield un-conservative results, especially for low heating rates.

The emphasis of thermal creep in steel structures has been recently recognized in previous studies [11–14]. These studies showed that time-dependent steel behavior depends on loading conditions along with fire exposure duration and magnitude. For example, Yang and Yu [14] observed time-dependent column buckling on *SN490FR* fire-resistant steel. Further, Torić et al. [8], as well as Kodur and Dwaikat [11], reached accurate predictions of deflection for thermally unrestrained beams, and axial force for restrained beams when thermal creep was explicitly included using Harmathy creep model [15]. El Ghor and Hantouche [16] conducted FE simulations including creep effects in isolated flush endplate connections exposed to fire temperatures. A methodology was developed to determine the creep behavior of the steel connection using isochronous curves. Although some research has been devoted to understanding time dependency (creep) of steel connections as an isolated connection, rather less attention has been paid to investigate the full-scale transient behavior of steel assemblies and to identify important time-dependent parameters affecting such behavior.

This study aims at including transient-state creep effects in identifying the different key parameters that affect the time-dependent behavior of shear endplate assemblies exposed to elevated temperatures. In the first part of this paper, FE models are developed using ABAQUS software [17] and validated against the experimental work performed by Wang et al. [4] at the University of Manchester. Then, a user-defined creep subroutine is developed and incorporated in the FE models [18]. The effect of key parameters such as heating rate, cooling rate, initial cooling temperature, load ratio, column size, column height, plate thickness, and steel grade is investigated. This research highlights the importance of including creep effects in the transient fire conditions for the sake of reaching a more accurate representation of the FE models. Disregarding creep may lead to unsafe design of steel structures, especially steel connections when exposed to elevated temperatures.

## 2. Constitutive Creep Models

Much research was done to study the creep behavior of steel at a material level [15, 19, 20]. However, not until recently, the material-specific creep properties were included in the numerical fire analysis of steel structures. For instance, Morovat [9] proposed an A992 steel creep model, whereas Wang et al. [19] proposed a Q460 high-strength steel creep model. Moreover, ASTM A36 steel creep models were developed by Harmathy [15] and Fields and Fields [20]. The creep model used in this study is the one proposed by Fields and Fields, which is widely used by researchers [3, 9, 13, 16]. Indeed, many trials on simple FE models were done to ensure that the subroutine is functioning well before applying it to more complex models, such as the ones presented in this study [18]. Fields and Fields empirical creep model represents the creep strain,  $\varepsilon_c$ , in the form of Norton-Bailey (power-law) equation as follows:

$$\varepsilon_c = at^b \sigma^c \quad (1)$$

where  $t$  is the time and  $\sigma$  is the stress, and  $a$ ,  $b$ , and  $c$  are parameters depending on material and temperature. This model predicts creep within a 350°C to 600°C temperature range and up to a 6% creep strain. Note that Fields and Fields model predicts both primary and secondary creep stages only. The tertiary stage is not analyzed in this study as it infers imminent failure. In this study, Fields and Fields creep model is incorporated as a user-defined subroutine in ABAQUS for both S275 and S355 steel. Since a constitutive creep model is limited to the type (grade) and chemical composition of steel, Luecke et al. [3] proposed a modification to Eq. (1) to account for thermal creep in different steel grades. When normalized to their ambient temperature values, tensile and yield strengths both follow a universal curve. Therefore, A36 steel creep models can predict the creep behavior in S275 and S355 steel when applying a certain scale by either yield or tensile strength ratios as shown:

$$\sigma_c = R_\sigma \sigma_a \quad (2)$$

where  $R_\sigma$  is the ratio of the yield or the tensile strength of steel, and  $\sigma_a$  is the applied stress. In this study,  $R_\sigma$  is taken as the ratio of the yielding strength of A36 to that of S355 or S275 steel. Since the Eurocode steel Grade S275 and the American steel Grade A36 share the same yielding strength, no stress modification is done to the subroutine regarding S275 material. On the contrary, the S355 material used in the large column is stronger than A36 steel, thus a modification in the subroutine is necessary. For S355 steel, the user-defined subroutine uses the corrected stress instead of the applied stress value when computing thermal creep.

The developed user-defined subroutine [18] is incorporated to calculate explicitly the creep strains in ABAQUS models. At the start of each increment, the subroutine is called to estimate the change in creep strain based on the instant stress, temperature, and creep strain history of each mesh element in the FE model and the conditions are assumed constant throughout the increment. To ensure its

accuracy, the proposed subroutine was tested on simple FE models before applying it to more complex models like the ones presented hereafter.

### 3. FE Modeling of Shear Endplate Connection Assemblies

FE models of shear endplate assemblies are developed using ABAQUS to reproduce the fire tests conducted at the University of Manchester [4]. Validating the FE models aims to ensure that they are yielding accurate and reliable results. This section briefly describes the geometry, material, and discretization of the structural elements, in addition to the analysis procedure regarding loads, boundary conditions, and temperature distribution.

#### 3.1. Assembly Geometry

The FE models of the two connection assemblies consist of a UB  $178 \times 102 \times 19$  beam of 2 meters length connected, using a  $150 \times 130 \times 8$  mm shear endplate, to two large columns (UC  $254 \times 254 \times 73$ ) in Test 2 and to two small columns (UC  $152 \times 152 \times 23$ ) in Test 7 both of height 3.67 meters. The endplate is bolted to the column flange and welded to the beam web. Four M20 tension bolts are used with standard size holes of a 20 mm diameter to avoid any convergence problems. Details of the shear endplate assembly of Test 2 are illustrated in Fig. 1.

#### 3.2. Material Properties

Different steel grades in the FE models are characterized by idealized bilinear stress–strain relationships. The beam, the shear endplate, and the small columns of Test 7 are of grade S275 steel while the large columns of Test 2 are of grade S355 steel. However, tensile coupon tests were done by Wang et al. [4] and showed slightly higher mechanical properties than those of S275 and S355. Further, structural bolts and nuts used are of Grade 8.8. The ambient mechanical properties used are summarized in Table 1 for each element. Note that the bolt threads are not modeled. Instead, a 25% reduction in bolt material strength, shown in Table 1, is applied to account for the bolt threads. Moreover, *Poisson's* ratio is taken 0.3 for all steel grades and temperatures. A reduction in the mechanical properties of structural steel and bolts at elevated temperatures is performed using retention factors presented by Lee et al. [21] and Hu et al. [22], respectively.

Although creep data in the steel material for temperatures exceeding  $600^{\circ}\text{C}$  are not available due to the limitation of the creep model used, creep was included in the validation up to  $800^{\circ}\text{C}$ . This is done to only evaluate the effect of creep in validating the FE models under experimental conditions (see Fig. 4a, b). For the sake of demonstration, the proposed method to account for that, is to assume the creep parameters for temperatures above  $600^{\circ}\text{C}$  equal to that of  $600^{\circ}\text{C}$ . In addition, the validations are also conducted while excluding creep in the material and a comparison with creep simulations and experimental results will be discussed later.

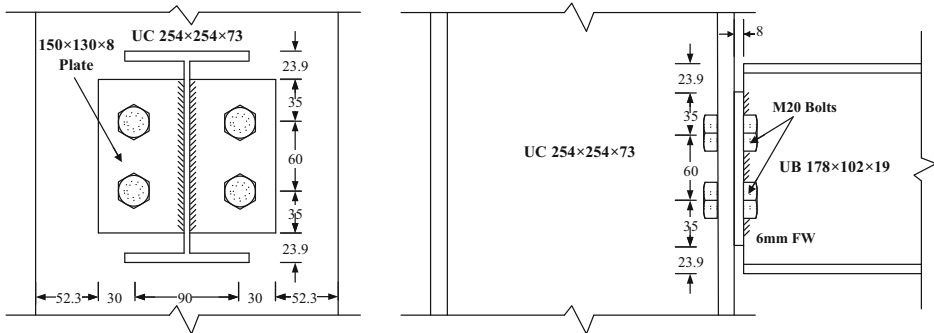


**Figure 1. Detailed geometrical configuration of the shear endplate connection with UC 254 × 254 × 73 column (in mm).**

**Table 1  
Ambient Mechanical Properties of the Assembly Components**

Ambient mechanical properties	Components				
	Beam	Endplate	Small column	Large column	Bolt
$E$ (MPa)	226,580	191,670	200,000	200,000	200,000
$F_y$ (MPa)	344	303	344	390	800
$F_u$ (MPa)	514	460	514	553	800

### 3.3. Model Discretization

Eight-node brick elements with reduced integration (C3D8-R) are used to discretize all assembly components. Bolts and their surrounding regions are discretized using a mapped meshing technique with finer mesh at the connection region where failure is most likely to occur. Further, the heads, shanks, and nuts of the bolts are modeled as cylinders. Slide, rotation, and separation of the surfaces in contact are allowed by applying a surface-to-surface contact having a temperature-independent friction coefficient of 0.25.

### 3.4. Applied Loads and Boundary Conditions

Since the assembly is symmetric about the beam mid-span, only half the frame is modeled with symmetry condition applied at the mid-span section of the beam. The first step assigned in the FE model is a pre-tensioning step followed by the loading phase where a 40 kN concentrated gravity load (representing a 0.5 load ratio) is applied 400 mm away from the symmetry axis. To avoid stress concentration, the 40 kN load is distributed as a pressure load on a small area.

The column ends are restrained horizontally, and the lower support is vertically restrained. A tie constraint is assigned between the shear endplate and the beam to represent the weld. Furthermore, the beam top flange is assigned a lateral dis-

placement restriction to represent the concrete slab restraining condition. Figure 2 shows the different details of the FE model.

A dissipated energy (artificial damping) technique is implemented in the FE models to mitigate convergence issues associated with high and rapid deformations at late stages of fire. A low dissipated energy fraction of  $10^{-5}$  is used to ensure accurate results and it is found to have a minor effect on the FE models outcome.

### 3.5. Temperature Profile

As reported by Wang et al. [4], difficulties to maintain uniform temperature distribution inside the furnace were encountered during the experiment. Further, the beam top flange was wrapped with an insulating material to mimic the heat-sink effect provided by the concrete slab. Therefore, to account for this non-uniformity in the temperature distribution, the FE model used for validation is divided into six areas each of which having a uniform temperature distribution. The regions, in increasing temperature order, are the unheated part of the column, the heated part of the column (400 mm panel zone), the beam top flange, the connection region, the beam web, and the beam bottom flange.

## 4. FE Model Versus Experimental Tests

The FE models results are validated against those of the experiment [4] to ensure that the FE models are yielding accurate and reliable predictions. As mentioned previously, two experiments on shear endplate connections (Tests 2 and 7) were conducted by Wang et al. [4], Test 2 involved large UC  $254 \times 254 \times 73$  column, while Test 7 involved a smaller one (UC  $152 \times 152 \times 23$ ). The validations are conducted while including and excluding creep in the material. The creep inclusion results for both column sizes indicate that creep has a little effect on the validation case of the FE models. Reasons for such effect include the fast heating rate; the thermal isolation of the beam upper flange, and the non-uniform heating of the assembly that delays the creep effects in less heated elements.

### 4.1. Large Column Model

In Test 2, difficulties were encountered during the experiment to maintain uniform heating between the left and the right side of the frame [4]. As reported, the connection at the right side completely fractured in shear at the toe of the weld, while the connection at the left side did not show any failure. The columns did not experience any local deformations. In the FE models, however, symmetry is considered in loading and heating, as discussed in the previous section. Figure 3 compares the connection's deformed shape of the experiment and the FE simulation at temperature  $750^\circ\text{C}$ . The FE model closely predicted the failure mode of the connection in the experiment since both show large shear endplate deformations. The dissipated energy fraction technique allowed continuing until the end of the heating stage. The severe stresses encountered in the FE model at the end of heat-

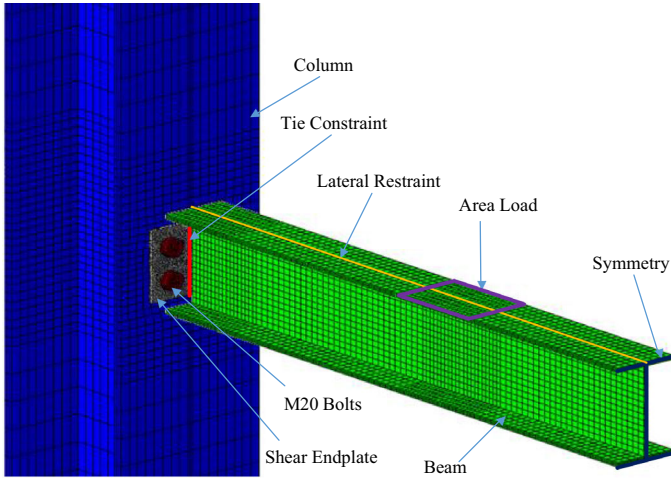


**Figure 2. Meshed finite element model assembly showing different geometrical restraints and boundary conditions.**

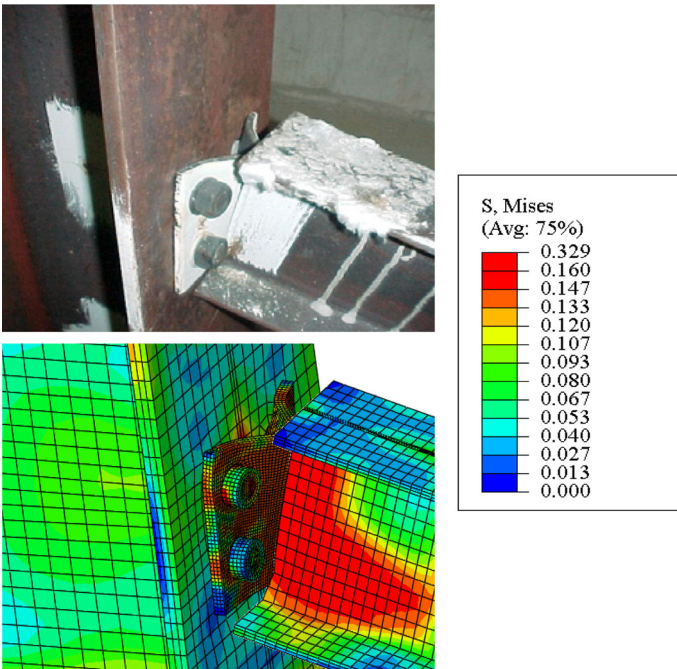


**Figure 3. FE and experimental deformation patterns for large column model (Test 2) [4].**

ing prevented the cooling stage initiation. Additionally, the FE model beam stresses were able to predict the complete shear failure of the beam web encountered on the right side of the experiment at the end of heating. The failure in the experiment caused constant deflections and axial forces during the cooling phase as shown in Fig. 4, which could not be modeled using the FE simulations. However, the parametric investigations, carried out later in the study, are limited to temperatures below 600°C, and the FE results until this temperature compared well with the experiment.

Figure 4a shows a good agreement between the results of the beam axial force of both the experiment and the FE model as a function of the beam lower flange temperature. As the temperature of the beam increases, the restraint provided by the column induces beam compressive forces. At 650°C, however, these forces start decreasing rapidly due to catenary action development. The same can be said when analyzing the mid-span deflection of the beam as shown in Fig. 4b. Both FE and experimental beam deflections increase slowly until 650°C where a rapid drop in deflection occurs as steel material faces more degradation. The small difference between the FE and the experimental results, shown in Fig. 4, is mainly due to the unsymmetrical heating in the experiment versus symmetric condition of heating in the FE model.

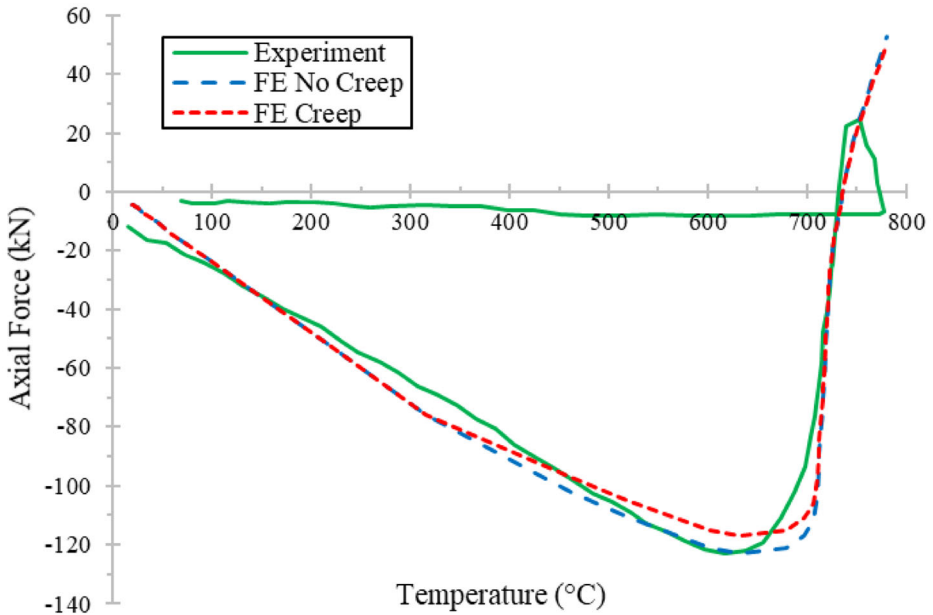
#### **4.2. Small Column Model**

Unlike Test 2, heating that is more symmetrical was achieved in Test 7, which helped in preventing shear failure of the beam web. However, due to the high flexibility of the column, the column flanges underwent significant distortions along with shear endplate bending in the experiment. This behavior is closely predicted by the FE model as shown in Fig. 5.

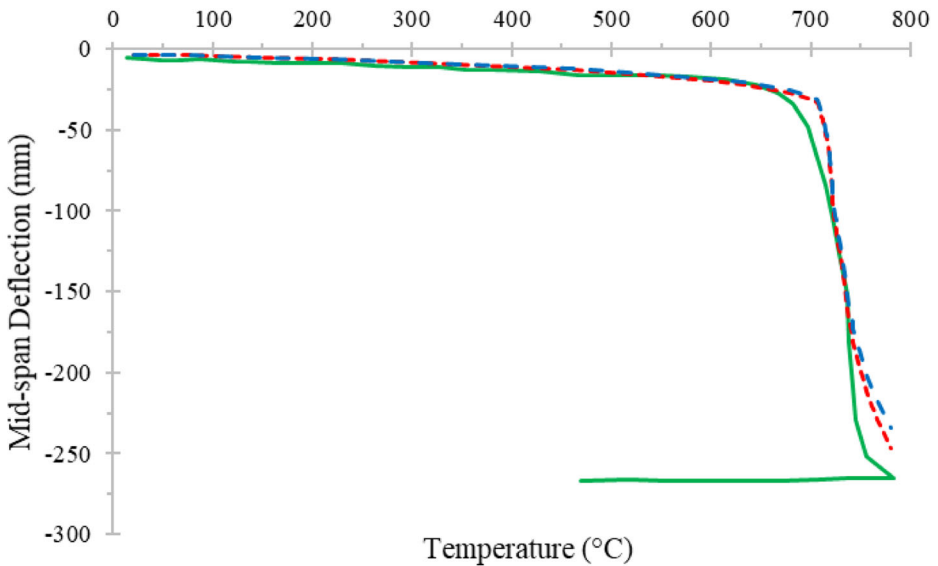
As for the axial force development in the beam, Fig. 6a shows reasonable agreement between experimental and FE model results until the temperature of nearly 700°C, where the axial force increases sharply until the analysis could not proceed further due to high shear endplate stresses. The same behavior is observed in Fig. 6b where the mid-span deflection of the experiment and FE models are in reasonable agreement. The experiment showed slight weld fracture, but such fracture cannot be predicted in the FE model due to the tie constraint used in the FE model instead of the weld. However, higher stresses are visualized at the shear endplate area in the FE model, and the difference between FE and experimental results is limited to 5%, which indicates a close prediction of the shear endplate behavior.

### **5. Effect of Key Parameters**

The effect of several parameters on the behavior of the shear endplate connection is investigated. These parameters are heating and cooling rate, initial cooling temperature, load ratio, column size, column height, plate thickness, and steel grade. Further, each parameter is analyzed while including thermal creep in order to study the time-dependent behavior of the assembly. In addition, the bolt size



(a)



(b)

**Figure 4. FE and experimental results for large column model (Test 2): (a) beam axial force; (b) mid-span deflection.**

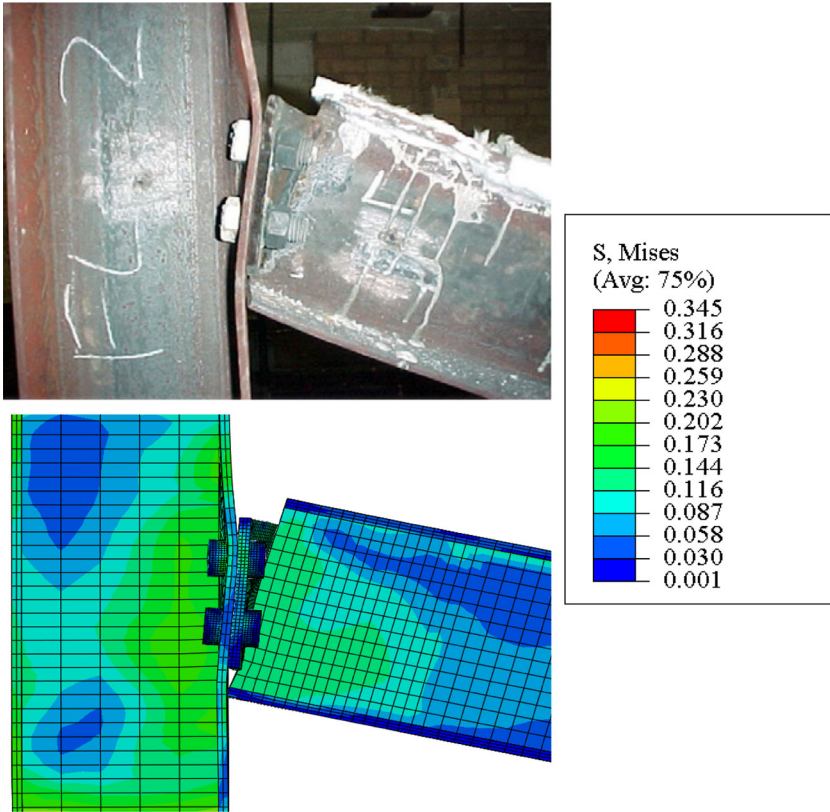
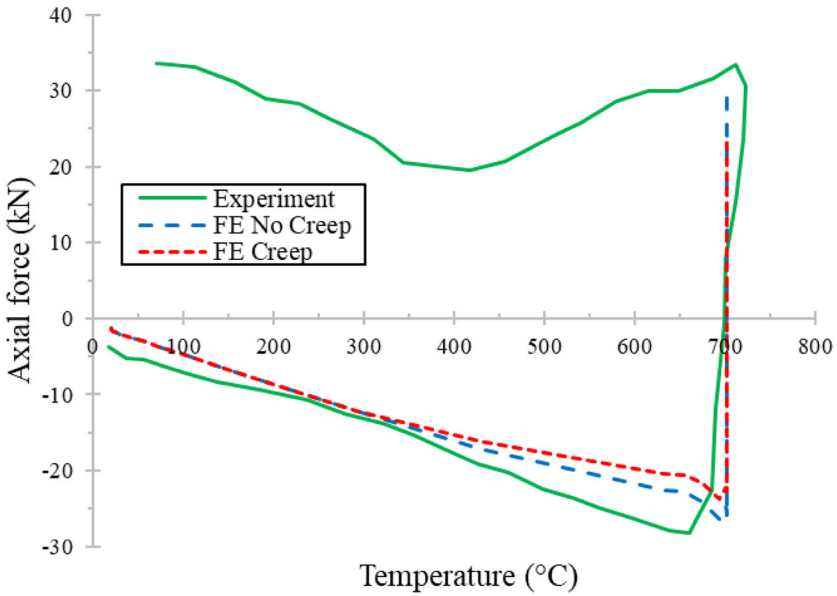


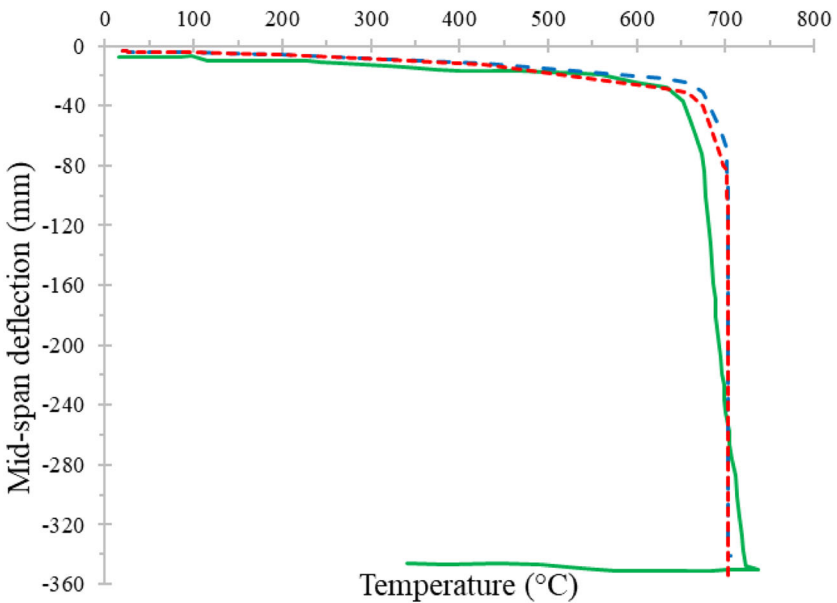
**Figure 5. FE and experimental deformation patterns for small column model (Test 7) [4].**

parameter proved to have no effect on the shear endplate assembly that is not shown in this study.

Some modifications are applied to the validated FE models. The load ratio for all models is kept as 0.5 represented by a point load of 40 kN unless otherwise specified. After the load application stage, a uniform temperature distribution is applied to all the heated regions of the assembly (400 mm of the column panel zone, connection region, and the whole beam). Then, the cooling stage followed a linear trend back to ambient temperature. In addition, since Fields and Fields creep model cannot predict creep at temperatures exceeding 600°C, this study is limited to a maximum temperature of 600°C. Thus, all the presented cases in this section have temperatures ranging between 20 and 600°C. A final note is that creep is applied to all the heated parts while considering the corrected stress for S355 steel grade according to Eq. (2). The dissipated energy fraction technique was not needed in the parametric studies since these models did not encounter any convergence problems.



(a)



(b)

**Figure 6. FE and experimental results for small column model (Test 7): (a) beam axial force; (b) mid-span deflection.**

### 5.1. Heating Rate

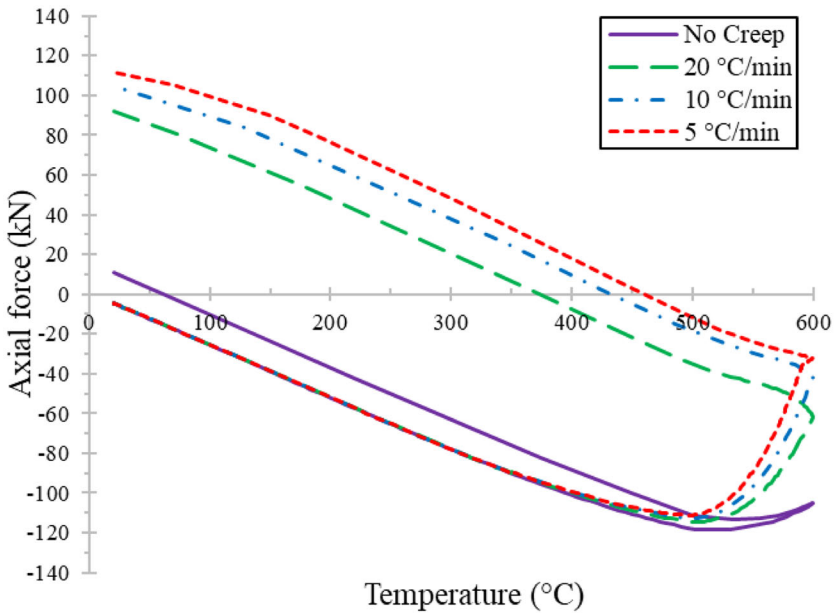
Depending on the fire scenario and whether the steel is protected or not, different heating rates may be present in the assembly. Consequently, fires can be classified from slow to fast heating. The rates analyzed are 5, 10, and 20°C per minute, including thermal creep. The time required for each to increase the temperature from 20 to 600°C is 116, 58, and 29 min, respectively. It should also be noted that the cooling phase included creep effect and had a cooling rate of 20°C per minute for the three heating rates.

Figure 7a represents the beam axial force versus temperature for all rates in addition to the case with no creep. It is observed that including creep causes a higher reduction in beam axial force after 500°C. Therefore, the beam tensile force at the end of the cooling phase is dependent on the heating rates such that the tensile force increases as the heating rate decreases. In the heating phase, failure is not observed in any of the models except for partial beam web yielding at the toe of the weld in all models. Furthermore, shear endplate yielding is observed when the cooling stage ended in the creep models. The extent of shear endplate distortion becomes more significant as the heating rate decreases. This excessive deformation and distortion lead to a contact between the beam bottom flange and the column flange just before the start of the cooling phase in the case of low heating rate (5°C per minute). As shown in Fig. 7b, the maximum deflection reached in the fast model (no creep) is about 12 mm, while it is 50, 64, and 76 mm for 5, 10, and 20°C per minute heating rates, respectively. Thus, including creep effect increases the deflection greatly and this increase is inversely proportional to the heating rate. Note that thermal creep effects take place between 350 and 600°C and more significantly after 500°C.

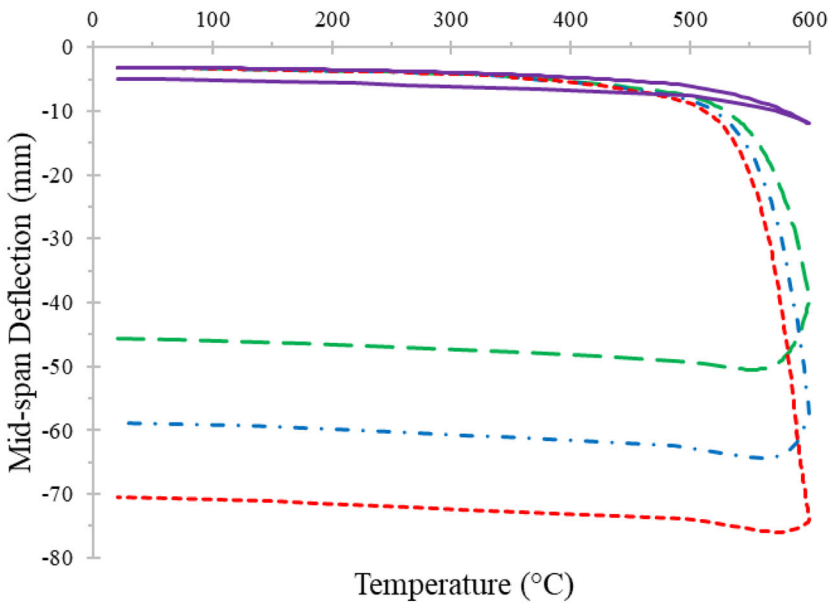
### 5.2. Cooling Rate

The effect of the cooling phase on the creep response of the connection assembly is investigated by varying the cooling rate. When reaching the decay phase of fire, many factors control the cooling rate of steel at which the steel temperature drops back to the ambient temperature. Three cooling rates are chosen: 5, 10, and 20°C per minute following one heating rate of 20°C per minute, and the results are shown in Fig. 8.

Having the same heating rate, all three cases reached the same axial force at the end of the heating phase then they diverge to reach different tensile forces at the end of the cooling phase. The maximum tensile force is observed in the lowest cooling rate (5°C per minute) as shown in Fig. 8a. Results from the analysis show that when lower heating rates preceded different cooling rates, the effect of changing cooling rates on the end axial force starts to diminish. Moreover, lower cooling rates expedite the effect of thermal creep on the beam and thus beam tensile forces and deflection gets even higher. Beam lower flange to column contact is also observed for the lowest cooling rate (5°C per minute) at the beginning of the cooling phase. By comparing values from Figs. 7b and 8b, it can be seen that the maximum deflections reached after cooling are nearly the same for reversed orders



(a)



(b)

**Figure 7. Heating rate effects including and excluding creep: (a) beam axial force; (b) mid-span deflection.**

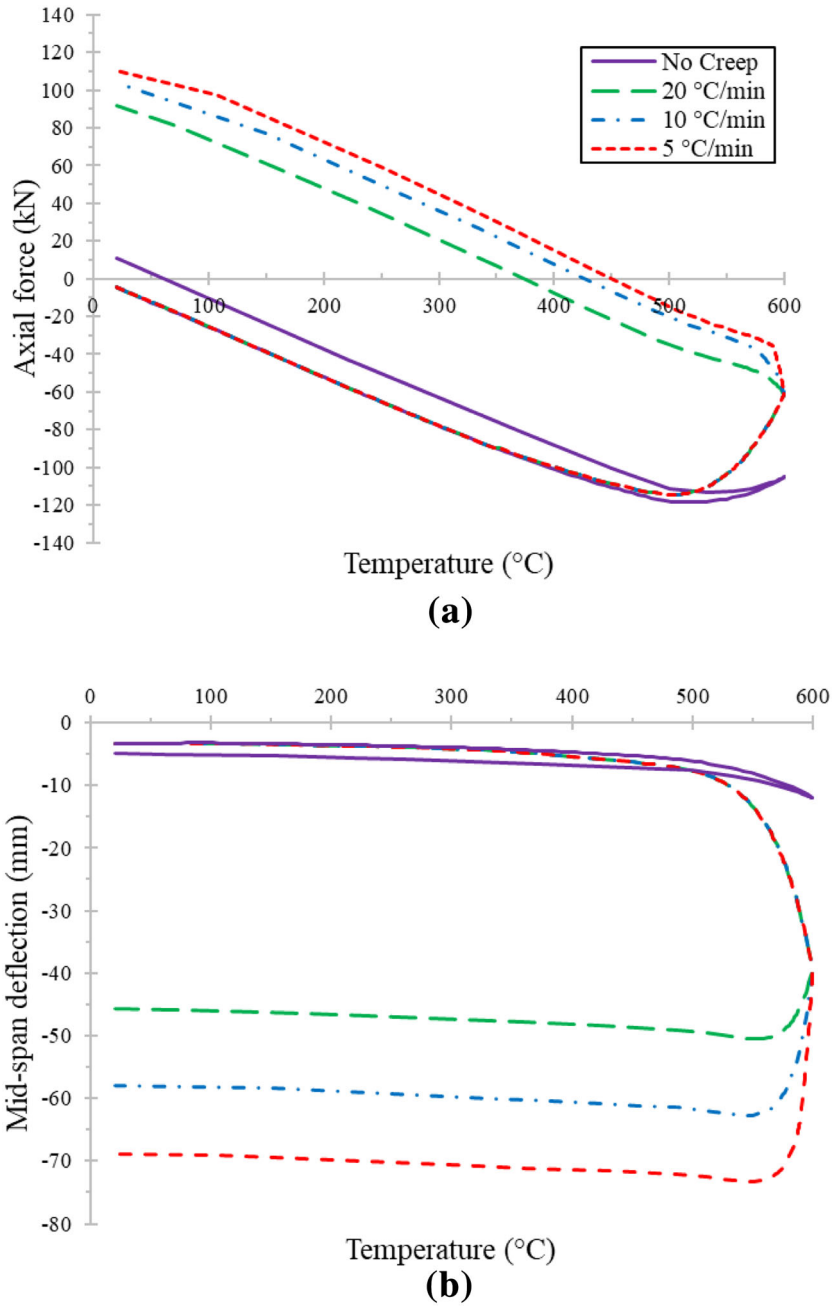


**Figure 8. Cooling rate effects including and excluding creep: (a) beam axial force; (b) mid-span deflection.**

of heating and cooling rates (5 then 20°C per minute compared to 20 then 5°C per minute).

### 5.3. Initial Cooling Temperature

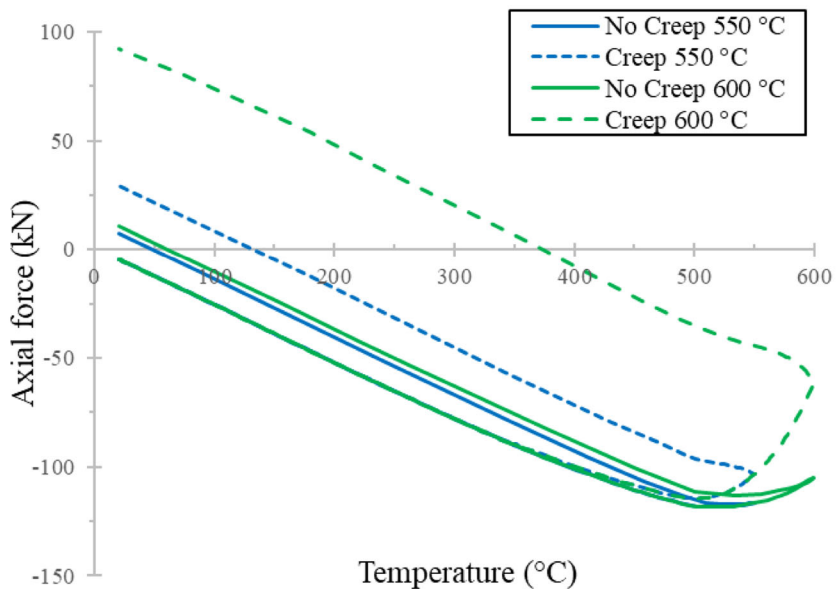
It was observed that connection failure occurs commonly during the cooling phase of fire because of the induced tensile forces [23]. The initial cooling temperature is the maximum temperature reached during a fire after which it drops back to the ambient temperature. Initial cooling temperatures analyzed are 450, 500, 550, and 600°C.

Figure 9a shows axial force in the beam versus temperature for the initial cooling temperatures of 550 and 600°C. As the initial cooling temperature increases, a larger tensile force development is produced at the end of the heating and cooling stages. This force increase is caused by the additional stiffness loss observed in the connection and beam as the temperature elevates. Figure 9b represents mid-span deflection of the beam as a function of temperature for the initial cooling temperatures of 550 and 600°C. When the initial cooling temperature increases, the deflection of the beam increases and the effect of thermal creep on displacement is also enlarged. This behavior is caused by the increase in stiffness loss of the beam at high temperatures, which causes sagging and leads to higher deflection. Furthermore, creep inclusion effects increase when the initial cooling temperature increases as observed in the vertical shift of curves sharing the same initial cooling temperature. This observation indicates that creep can be neglected for initial cooling temperatures below 500°C but is significant after this temperature. For that reason, 450 and 500°C models are not shown in Fig. 9. In all cases, no failure has occurred.

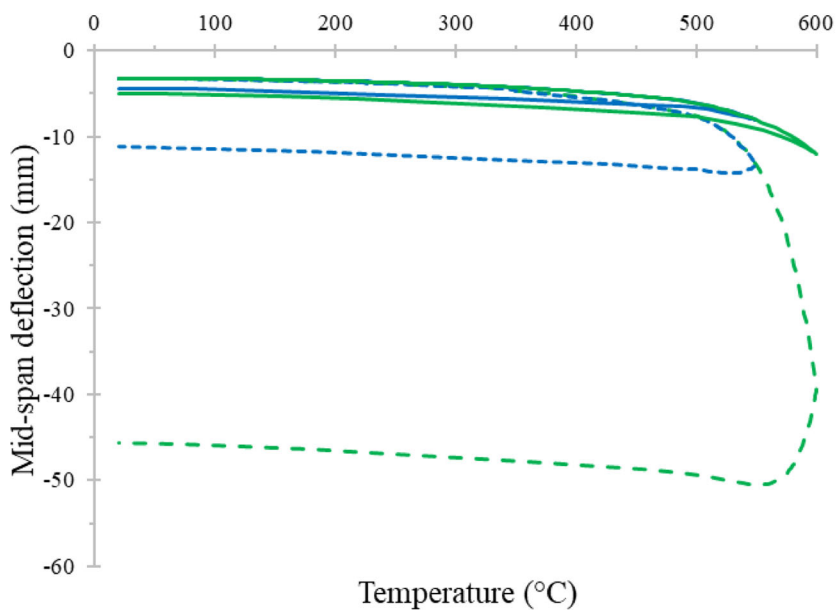
### 5.4. Load Ratio

The load ratio is defined as the ratio of the maximum moment generated in the beam, due to the applied concentrated loads, to the nominal plastic moment capacity of the beam section,  $M_p$ , at ambient temperature. Assuming pin connection behavior, the maximum moment developed at the beam mid-span is computed as  $P \times a$  where  $P$  is the concentrated point load applied and  $a$  is the distance from the face of the column to the point load (600 mm). The load ratios are chosen to be 0.33, 0.5, and 0.67 corresponding to point load magnitudes of 26.7, 40, and 53.3 kN, respectively. Also, note that the nominal plastic moment capacity of the beam is calculated for S275 material whereas tensile coupon tests revealed an average yield stress of 345 N/mm<sup>2</sup>, which means that the true load ratios are expected to be less than the specified.

Axial force versus beam temperature for the different load ratios with and without thermal creep inclusion is shown in Fig. 10a. No significant variation of the beam axial force during either heating or cooling phases is observed in the case of load ratios of 0.33 and 0.5 excluding creep. However, when creep is included in these two load ratios, a greater difference in tensile axial force is observed. Further, the analysis shows that higher load ratios produce less compressive forces in the beam and higher tensile forces after the catenary action. It is also observed



(a)



(b)

**Figure 9. Initial cooling temperature effects including and excluding creep: (a) beam axial force; (b) mid-span deflection.**

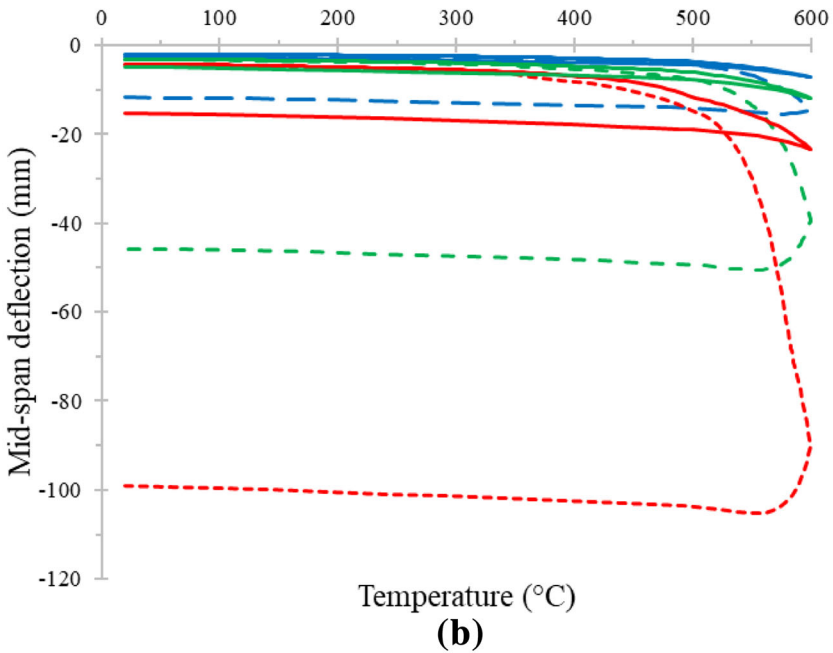
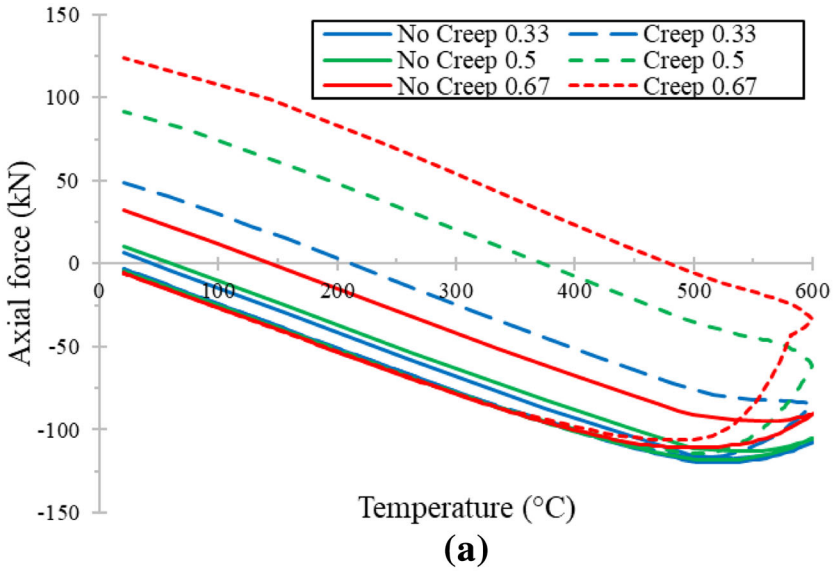
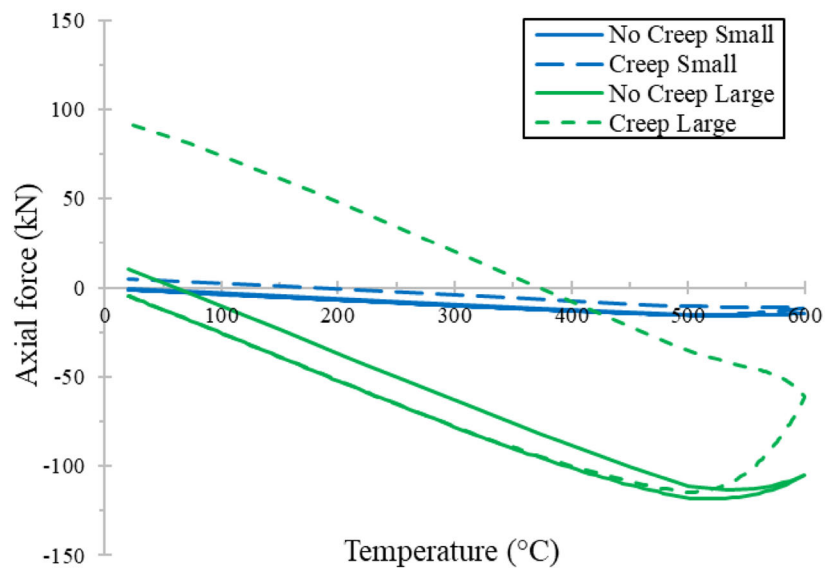
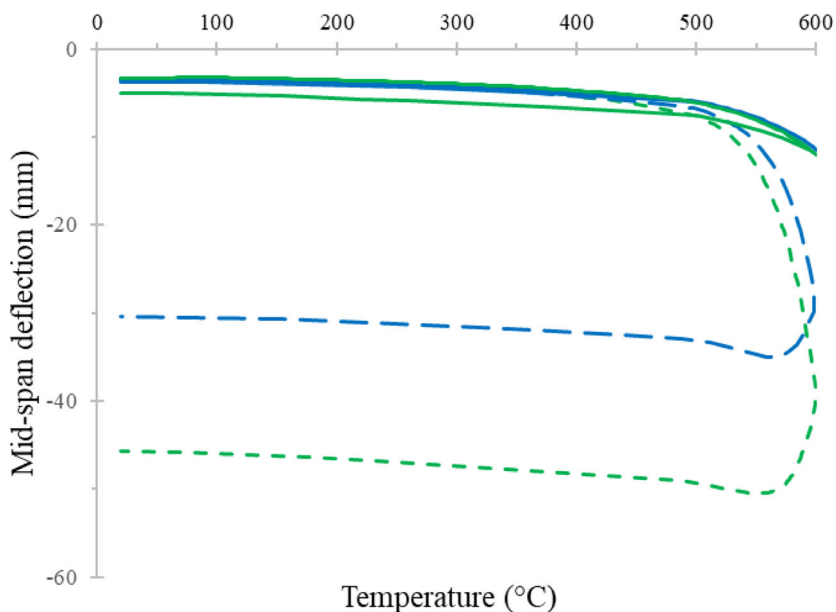


**Figure 10. Load ratio effects including and excluding creep: (a) beam axial force; (b) mid-span deflection.**



(a)



(b)

**Figure 11. Column size effects including and excluding creep: (a) beam axial force; (b) mid-span deflection.**

that the difference in tensile forces between models including and excluding thermal creep gets higher when the load ratio is increased. This can be attributed to the increase in beam stresses caused by the increase in load ratio, which directly augments thermal creep strain development. For the models of load ratio 0.33, whether creep is included or not, no sign of yielding is observed. On the contrary, the model of 0.67 load ratio excluding creep shows beam web yielding near the weld, top flange yielding between the load and mid-span, and partial shear endplate yield at a temperature of 480°C. Whereas the model of 0.67 load ratio including creep shows the same yielding of the three zones but at a delayed temperature of 520°C. This delaying is a result of axial stress relaxation caused by creep. In addition, significant shear endplate yielding is observed at the end of cooling for the 0.67 model with creep due to the large tensile force as Fig. 10a represents. Figure 10b shows beam mid-span deflection for the different ratios. The same can be said regarding the effects of both load ratio and creep inclusion in different load ratios where the deflection is far more amplified.

### 5.5. Column Size

The flexural stiffness of the columns provides axial restraint on the beam's end. The column size (cross-section) is one of the main factors that control the flexural stiffness of a column. The two models of large (UC 254 × 254 × 73) and small (UC 152 × 152 × 23) column sizes previously used are now studied at uniform heating of 600°C with and without thermal creep inclusion. The creep is included in both heating and cooling stages with a rate of 20°C per minute and the columns are of the same height (3.67 m).

As expected, the large column model allows the beam to develop more axial force than the small column model due to the higher flexural stiffness of the column that imposes a higher axial restraint on the beam as presented in Fig. 11a. It can also be seen that creep inclusion caused an 82 kN and 5 kN increase in the tensile force at the end of cooling for the large and the small column models, respectively. This difference is due to the large axial force on the beam seen in the large column model that magnifies thermal creep effects, as stress is a controlling factor of creep strain development. Furthermore, no sign of yielding is detected in the small column model (with and without creep). As for the mid-span deflection represented in Fig. 11b, the two models without creep have nearly the same deflection. Nevertheless, when the thermal creep is included, a large difference in deflection is observed as shown in the large column model due to the higher stresses as discussed earlier.

### 5.6. Column Height

The two column heights considered in this analysis are composed of the same column section (UC 254 × 254 × 73) and are classified into long (3.67 m) and short (2.45 m) columns. The columns in both models had the same heated region of 400 mm height next to the connection and the ratios between the height of the columns above and below the beam are conserved. The two cases are studied with and without the effects of thermal creep.

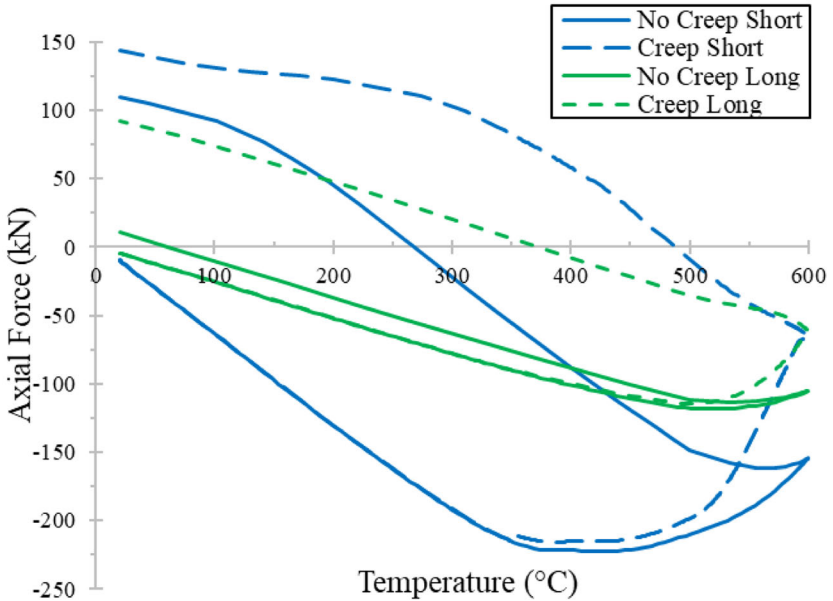
Axial compressive forces developed in the beam for the short column models are about double the axial compression in the long column models as can be seen in Fig. 12a. However, creep inclusion in both models lead to increased tensile forces where the short column model develops more tension in the beam than the long column model does. Also, contact between the beam lower flange and the column flange is observed just before cooling in the short column creep model. This contact is due to the higher induced axial load on the beam that leads to premature yielding, sagging, and eventually beam-column contact. The short column model excluding creep showed beam web yielding near the weld at 340°C followed by top flange yielding between the load and mid-span at 420°C. Whereas the short column model including creep showed the same two yielding behaviors but at a delayed temperature (380°C for beam web and 470°C for top flange). In addition, for the short column, shear endplate yielding is observed at the end of cooling for models with and without creep but yielding in the creep model is far more significant. By comparing the deflections of the short and long column models, Fig. 12b shows more deflection for the short column when creep is excluded but nearly equal deflections when creep is included. This equality can be explained by the contact observed in the short column model with creep, which increasingly restrained further deflection of the beam. Thus, deflection in the short column model did not develop and became nearly equal to the deflection in the long column model including creep.

### 5.7. Shear Endplate Thickness

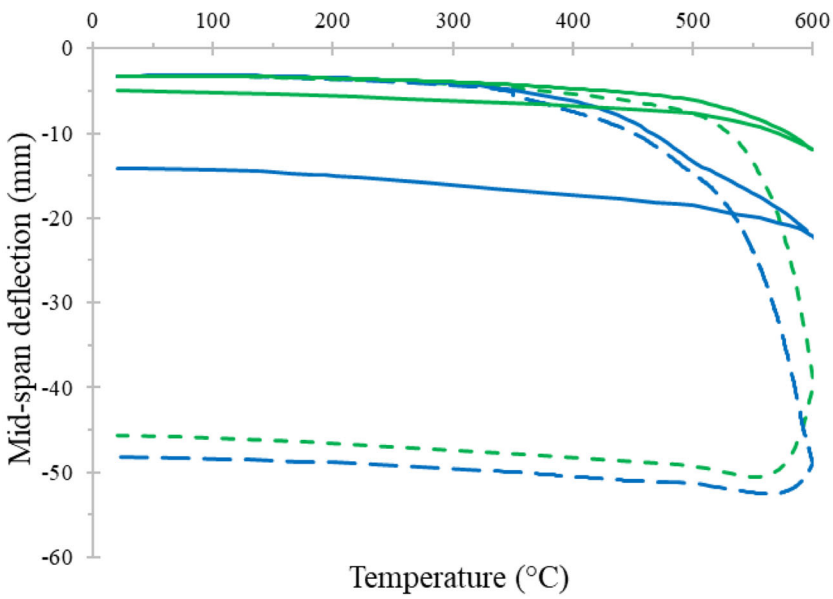
Three endplate thicknesses of 8, 10, and 12 mm are considered with and without including creep. As expected, beam tensile axial force where thermal creep is included showed an increase at the end of the heating and cooling phases as presented in Fig. 13a. However, no significant change in axial force is recorded for the different shear endplate thicknesses except for a slight increase in tensile force as thickness increases in the creep inclusion models. This slight increase is due to the increase in the endplate stiffness allowing additional force in the beam to develop. In addition, the shear endplate yielding observed in the previous creep models at the end of the cooling stage diminished when the thickness of endplates is increased to 10 and 12 mm. As for mid-span deflection shown in Fig. 13b, as thicknesses increase in the creep models, the deflection of the beam decreases slightly which is a result of the increased rotational stiffness of the shear endplate. In conclusion, the effect of varying the shear endplate thickness on the assembly behavior can be considered minor.

### 5.8. Steel Grade

Creep strain development is influenced by the grade of steel utilized in the analysis. As stated before, for steel grades other than S275, this study uses the modified Fields and Fields creep model, which was proposed by Luecke et al. [3]. It employs the *corrected* stress in calculating the incremental creep strains in the analysis. To investigate the effect of steel grade on the time-dependent behavior of the assembly, three cases of different steel grades, are compared under the same

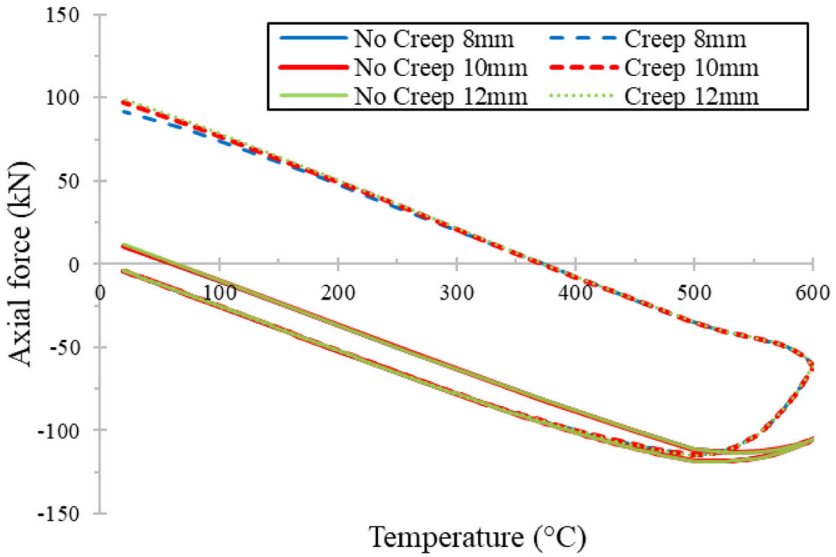


(a)

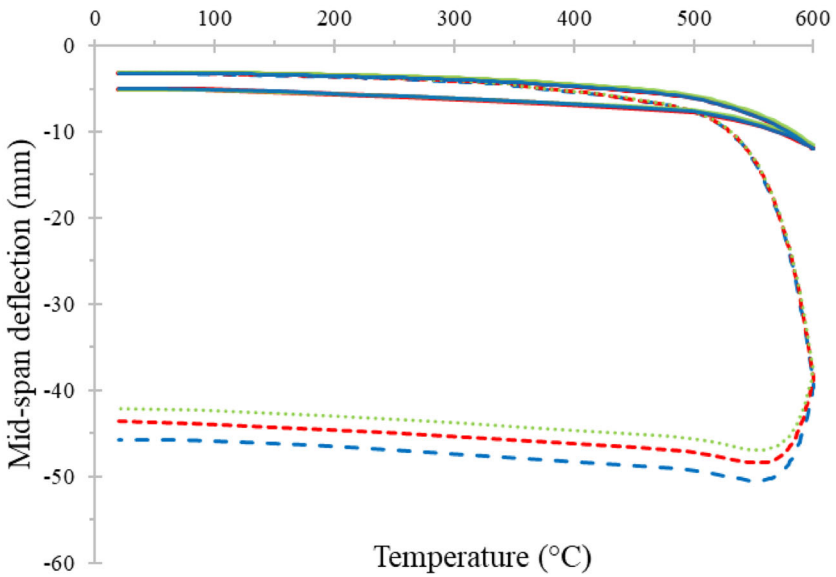


(b)

**Figure 12. Column height effects including and excluding creep: (a) beam axial force; (b) mid-span deflection.**



(a)



(b)

**Figure 13. Endplate thickness effects including and excluding creep: (a) beam axial force; (b) mid-span deflection.**

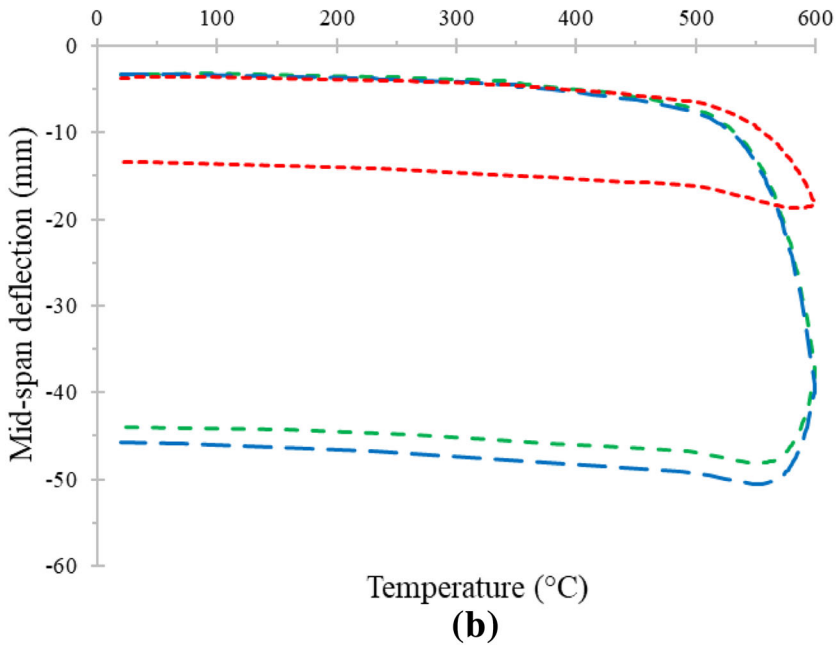
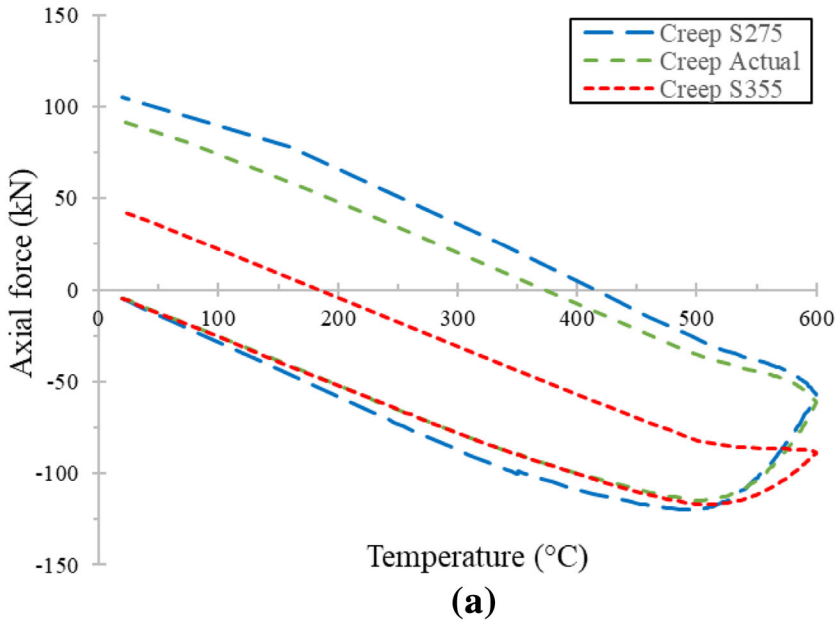


**Figure 14. Steel grade effects including creep: (a) beam axial force; (b) mid-span deflection.**

heating and cooling rates of 20°C/min. The cases are (1) the actual case with the beam of steel grade S275 and the column of steel grade S355, (2) both the beam and column are of steel grade S275, and (3) both the beam and column are of steel grade S355. The results are shown in Fig. 14. Although there is still a creep effect for steel grades higher than S275, the impact of creep in S355 is greatly reduced to nearly half when compared to S275 creep. The actual case where the beam is S275 and the column is S355 is closer to the case where both beam and column are S275. This is because the assembly is more sensitive to the change of beam material rather than the column since the beam is the main component that is subjected to fire. In conclusion, it is clearly shown that using a higher steel grade may reduce the creep impact on the connection behavior in fire.

## 6. Conclusions

This paper summarizes a numerical study on the thermal creep behavior of shear endplate assemblies due to the transient state of fire. The FE simulations have proven to predict the strength and deformation response of the shear endplate connection accurately, in spite of the absence of fracture modeling that prevented the cooling stage initiation after the failure of the first component. Creep is explicitly included, through a user-defined subroutine, to investigate the time-dependent effects on the strength and flexibility of shear endplate connections. Beam axial forces and mid-span deflections versus temperature are the two criteria used to describe the response of the assembly exposed to fire temperatures.

The FE models presented in this paper show that mid-span deflection increase and axial stress relaxation can be significant for high temperatures, high stresses, and long fire exposure durations when considering thermal creep. This behavior emphasizes that ignoring thermal creep may cause underestimation of beam deflections and overestimation of beam thermally induced axial forces, which leads to unsafe design of beam-column steel connections exposed to elevated temperatures. More specifically, the behavior of shear endplate connections depends extremely on time for temperatures that exceed 500°C according to the Fields and Fields creep model used. The results show that the influence of thermal creep is inversely proportional to the heating and cooling rates. Therefore, it is essential to account for time-dependent effects when designing steel connections exposed to long durations of fire (e.g. thermally protected steel).

When slower heating precedes cooling, the effect of varying cooling rates on the beam behavior diminishes. Thus, the effect of creep is not a function of either cooling or heating rates independently, but in fact, a function of their interaction. In severe conditions, such as high load ratios and low rates of heating, thermal creep can alter the behavior of the beam-column connection by redistributing stresses between supporting regions. The parametric studies show that some parameters such as heating and cooling rates, initial cooling temperature, load ratio, column size, and column height greatly affected the time-dependent behavior of the connection. On the other hand, connection configuration, such as end-

plate thickness and bolt diameter, has a small effect on the overall time-dependent behavior of the assembly.

To enhance the accuracy of the fire analysis, the development of creep models for different components, temperature ranges, and steel compositions is crucial. Creep models for both bolts and welds should be developed since the current studies including creep are still unable to predict the effect of creep in such elements, which might play a major role when studying connection configurations for a given assembly. In addition, this study shows that the material for which the fire tests are conducted can play a major role in influencing the creep behavior. This highlights the necessity of also performing creep tests on various steel grades and chemical compositions. In spite of the approximate proposed way in overcoming the temperature limit in the used creep model, more reliable creep models need to be developed to include creep effect at temperatures larger than 600°C. Thus, experimental and analytical work investigating the three above-mentioned limitations are necessary for future research in this field.

Although FE modeling is a reasonably accurate method, it has the drawback of high computational cost. Therefore, future work should be carried out to develop a mechanical-based model, a less computational cost alternative, based on the conclusions of this research such as the main parameters affecting time-dependent behavior of shear endplate connections. The mechanical model could be used as a practical tool for designing steel connections subjected to elevated temperatures.

## References

1. Ramli-Sulong NH, Elghazouli AY, Izzuddin BA (2007) Behaviour and design of beam-to-column connections under fire conditions. *Fire Saf J* 42(6–7):437–451. <https://doi.org/10.1016/j.firesaf.2006.09.003>
2. Bailey CG, Burgess IW, Plank RJ (1996) Analyses of the effects of cooling and fire spread on steel-framed buildings. *Fire Saf J* 26(4):273–293. [https://doi.org/10.1016/S0379-7112\(96\)00027-6](https://doi.org/10.1016/S0379-7112(96)00027-6)
3. Luecke WE, McColskey JD, McCowan CN, Banovic SW, Fields RJ, Foecke TJ, Siewert TA, Gayle FW (2005) Federal building and fire safety investigation of the world trade center disaster: mechanical properties of structural steels
4. Wang YC, Dai XH, Bailey CG (2011) An experimental study of relative structural fire behaviour and robustness of different types of steel joint in restrained steel frames. *J Constr Steel Res* 67(7):1149–1163. <https://doi.org/10.1016/j.jcsr.2011.02.008>
5. Hu Y, Davidson B, Burgess I, Plank R (2008) Experimental study on flexible end plate connections in fire. In: Proceedings of 5th European conference on steel structures, Graz, Austria, pp 1007–1012
6. Hantouche EG, Sleiman SA (2016) Response of double angle and shear endplate connections at elevated temperatures. *Int J Steel Struct* 16(2):489–504. <https://doi.org/10.1007/s13296-016-6019-8>
7. Hantouche EG, Sleiman SA (2017) Axial restraint forces in shear endplates of steel frames due to fire. *J Constr Steel Res* 128:528–541. <https://doi.org/10.1016/j.jcsr.2016.09.021>

8. Torić N, Harapin A, Boko I (2013) Modelling of steel creep at high temperatures using an implicit creep model. *Key Eng Mater* 553:13–22. <https://doi.org/10.4028/www.scientific.net/KEM.553.13>
9. Morovat MA (2014) Creep buckling behavior of steel columns subjected to fire. Dissertation, The University of Texas at Austin
10. EN 1993-1-2 (2005) Eurocode 3: design of steel structures—part 1–2: general rules—structural fire design, European Committee for Standardization, Brussels
11. Kodur VR, Dwaikat MM (2010) Effect of high temperature creep on the fire response of restrained steel beams. *Mater Struct* 43(10):1327–1341. <https://doi.org/10.1617/s11527-010-9583-y>
12. Li G, Zhang C (2012) Creep effect on buckling of axially restrained steel columns in real fires. *J Constr Steel Res* 71:182–188. <https://doi.org/10.1016/j.jcsr.2011.09.006>
13. Morovat MA, El Ghor AH, Hantouche EG (2018) Time-dependent response of flush endplate connections to fire temperatures. *J Struct Eng* 144(4):04018023. [https://doi.org/10.1061/\(ASCE\)ST.1943-541X.0002006](https://doi.org/10.1061/(ASCE)ST.1943-541X.0002006)
14. Yang K, Yu Z (2013) Experimental research on the creep buckling of fire-resistant steel columns at elevated temperature. *Steel Compos Struct* 15(2):163–173. <https://doi.org/10.12989/scs.2013.15.2.163>
15. Harmathy TZ (1967) A comprehensive creep model. *J Basic Eng* 89(3):496–502. <https://doi.org/10.1115/1.3609648>
16. El Ghor AH, Hantouche EG (2017) Thermal creep mechanical-based modeling for flush endplate connections in fire. *J Constr Steel Res* 136:11–23. <https://doi.org/10.1016/j.jcsr.2017.04.022>
17. Abaqus Ver. 6.14 Documentation (2014) Dassault Systemes Simulia Corporation
18. Hantouche EG, Al Khatib KK, Morovat MA (2018) Modeling creep of steel under transient temperature conditions of fire. *Fire Saf J* 100:67–75. <https://doi.org/10.1016/j.firesaf.2018.07.006>
19. Wang W, Yan S, Liu J (2017) Studies on temperature induced creep in high strength Q460 steel. *Mater Struct* 50:68. <https://doi.org/10.1617/s11527-016-0941-2>
20. Fields AB, Fields JR (1989) Elevated temperature deformation of structural steel. National Bureau of Standards NISTIR 88-3899
21. Lee J, Morovat MA, Hu G, Engelhardt MD, Taleff EM (2013) Experimental investigation of mechanical properties of ASTM A992 steel at elevated temperatures. *Eng J* 50:249–272
22. Hu Y, Davison BJ, Burgess WI, Plank RJ (2007) Comparative study of the behaviour of BS 4190 and BS EN ISO 4014 bolts in fire. In: Proceedings of 3rd international conference on steel and composite structures (ICSC07), pp 587–592
23. Garlock EM, Selamet S (2010) Modeling and behavior of steel plate connections subject to various fire scenarios. *J Struct Eng* 136(7):897–906. [https://doi.org/10.1061/\(ASCE\)ST.1943-541X.0000179](https://doi.org/10.1061/(ASCE)ST.1943-541X.0000179)